Materials Research. 2019; 22(3): e20180689
DOI: http://dx.doi.org/10.1590/1980-5373-MR-2018-0689

Co_3O_4-ZnO P-N Heterostructure Nanomaterials Film and its Enhanced Photoelectric Response to Visible Lights at Near Room Temperature

Nan Han[a], Guofeng Pan[a], Jie Zheng[a], Ru Wang[a], Yudong Wang[b]*

[a]*Key Laboratory of Electronic Materials and Devices of Tianjin, School of Electronics and Information Engineering, Hebei University of Technology, Tianjin 300130, PR China*
[b]*School of aerospace engineering, Beijing Institute of Technology, Beijing 100081, P R China*

Received: October 23, 2018; Revised: January 04, 2019; Accepted: March 09, 2019

In this paper, Co_3O_4-ZnO nanomaterials with Co_3O_4 doping mass fractions of 0%, 2.13%, 4.13%, and 6.13% were prepared by sol-gel method. In order to explain and confirm the influence of the incorporation of Co_3O_4 on the surface morphology and gas sensitivity of ZnO at a relatively low gas concentration, additional studies such as XRD, XPS, SEM, EDS and UV-vis spectroscopy were performed. And its photoelectric response to 100 ppm acetone at near room temperature and visible light irradiation was studied. Due to the formation of P-N heterojunctions, the Co_3O_4-ZnO heterostructural nanoparticles has a highe response to low concentrations of acetone gas than undoped ZnO nanoparticles even at operating temperatures as low as 30ºC. The addition of Co_3O_4 improves the sensitivity and selectivity of ZnO thick films. The sensitivity of the 4.13wt% Co_3O_4-ZnO sample to 100 ppm acetone at a working temperature of 30ºC was 24.36. The light excitation effect was significantly enhanced. Under visible light irradiation, the sensitivity can reach 37.21. In addition, the Co_3O_4-ZnO P-N heterojunction model was combined with visible light excitation theory to further explore the mechanism of gas sensing reaction.

Keywords: *Zinc oxide, Acetone, Photoelectric response, Gas sensitivity, Heterojunction.*

1. Introduction

Metal oxide semiconductor materials have attracted wide attention from researchers as sensitive materials for detecting toxic and harmful gas [1]. Among these materials, zinc oxide is one of the earliest discovered and widely studied materials. which is a typical wide band gap n-type direct band gap semiconductor material with lower resistivity and higher light trapping properties [2].Due to zinc oxide's wide band gap (3.37 eV at room temperature), it is necessary to increase the operating temperature to obtain better gas sensing characteristics, usually 250 to 400ºC. However, high temperatures not only lead to high power consumption, but also limit the detection of flammable and explosive gases, and it is also a challenge to the stability of the device [3,4]. Therefore, in order to lower the operating temperature of the sensor and increase the sensitivity, a large number of scientific papers on the use of zinc oxide as a gas sensor have been published. For example, many of precious metal elements, rare earth elements or metal compounds were doped into zinc oxide. The preparation of Tb-doped zinc oxide samples by Anita Hastir et al. significantly improved the sensitivity to ethanol and acetone [5]. Qi Xu's Cu-doped ZnO nanorods prepared by the hydrothermal method have a response of 8 to 50 ppm TEA at a low temperature of 40ºC, and the response time and recovery time are 5 s and 25 s, respectively [6]. A.P. Rambu et al. used magnetron sputtering deposition to obtain 3% (mass fraction) Co doped ZnO nanofibers [7]. The best operating temperature for 600 ppm methane was 170ºC and the sensor was stable for a long time. Moreover, the formation of semiconductor heterostructures has been proven to be an effective way to improve gas-sensing properties, such as sensitivity and especially lower operating temperatures. For example, wang et al. synthesized CuO/ZnO nanorod hybrids have a sensitivity of up to 40 for 100 ppm H_2S at a working temperature of 100ºC [8]. Xing Gao et al. reported that Co_3O_4-ZnO core-shell heterostructure NFs can detect 100 ppm of formaldehyde gas at 220ºC [9].

In addition, a large number of studies have found that UV radiation can greatly reduce the operating temperature of the sensor, leading to improved performance of ZnO-based photoelectric gas sensors. However, there are few articles on the application of visible light to ZnO gas sensors. Therefore, the improvement of the gas-sensitivity of zinc oxide sensors by visible light is one of the focuses of this experiment.

In this paper, different cobalt-doped precursors were prepared by simple sol-gel method, and different doped zinc oxide powder samples were produced by high temperature treatment. The effects of cobalt doping on the crystal structure and morphology of zinc oxide were investigated. The role of P-N heterojunction in sensor signal formation was analyzed, and the influence of visible light excitation on the gas sensitivity of CZO was studied. The mechanism of gas-sensing reaction was further explored.

*e-mail: pgf@hebut.edu.cn.

2. Experimental

2.1 Co-doped ZnO composites and devices

A source of $Zn(CH_3COO)_2 \cdot 2H_2O$, NaOH, $CoCl_2.6H_2O$ as a raw material. Different ratios of zinc acetate and cobalt chloride were dissolved in a mixture of anhydrous ethanol and deionized water in equal proportions. An aqueous NaOH solution was prepared, and an aqueous NaOH solution was slowly added to a mixed solution of cobalt chloride and zinc acetate until the pH was equal to 7, and then the sol was obtained by magnetic stirring at room temperature. The stirring speed was 100r/min and the stirring time was 2h. The sol was aged at room temperature for 24 hours, the sample was placed in an 80ºCinfrared oven and dried to obtain gel. The gel was ground, washed and annealed to finally obtain Co_3O_4-ZnO powder. In the current work, we prepared four different doping amounts of ZnO powder, respectively 0 wt%, 2.13 wt%, 4.13 wt%, and 6.13 wt%.

To make a thick-film sensor, the above samples were each added with a proper amount of deionized water to each agate mortar, and then ground for about 10 minutes to form a paste. Dipping method was used to prepare different heat-dosed thick-film type gas sensors on the surface of Al_2O_3-based ceramic tube.

2.2 Characterization of ZnO films

The crystal structure of Co_3O_4-ZnO was analyzed by X-ray diffraction (XRD, Bruker AXS D8 FOCUS, Germany) with Cu-Kα1 radiation (λ =1.5406 Å) in the 2θ range of 20º-80º with 0.02º/s scanning step. The microstructures were analyzed by scanning electron microscopy (SEM, ZEISS Sigma500, Germany). The element surface distribution of Zinc oxide and cobalt were determined by Oxford X-MaxN150 EDS. Chemical binding analysis was conducted by an X-ray photoelectron spectrograph (XPS, ESCALAB MKK II) operated using Mg as the exciting source. The diffuse reflectance spectra of pure ZnO and 4.13wt% Co_3O_4-ZnO were measured by UV-vis spectrophotometer (Shimadzu, UV-2600, Japan) with a scanning range of 220-850 nm and a scanning speed of 0.5 nm /s.

2.3 Gas sensing properties testing

In this work, the sensitivity of the gas sensors was tested with the HW-30B gas sensor test system.The schematic of test circuit was shown in Fig. 1.

In the above circuit, Vh represents the voltage of the heating circuit, which controls the working temperature.Vc is the circult voltage, Vout is the output voltage, and R1 is the load resistance that matches the component resistance. In this experiment, the gas detection is completed by taking a change in resistance when the sensor is in contact with the detected gas. Thesensitivity is defined as S.

$$S = R_a / R_g \quad (1)$$

R_a is the resistance of sensor in air; R_g is the resistance of sensor in target gas.

3. Result and Discussion

3.1 Structure and morphology

The crystal structure of Co_3O_4-ZnO was analyzed by X-ray diffraction (XRD). The XRD pattern of the different sample materials is shown in Fig. 2. All diffraction peaks can point to hexagonal (wurtzite) ZnO, which is well consistent with the JCPDS: #36-1451. In addition, the peak areas and intensities of the four samples vary with the different doping amount of Co_3O_4. The strong and sharp diffraction peak of 4.13wt% Co_3O_4-ZnO indicates that the product has high crystallinity[10]. The characteristic diffraction peak of the cobalt oxide crystal wasn't detected by XRD experiment ,and possible reason is that the content of Co_3O_4 in the sample is too low to be detected[11].

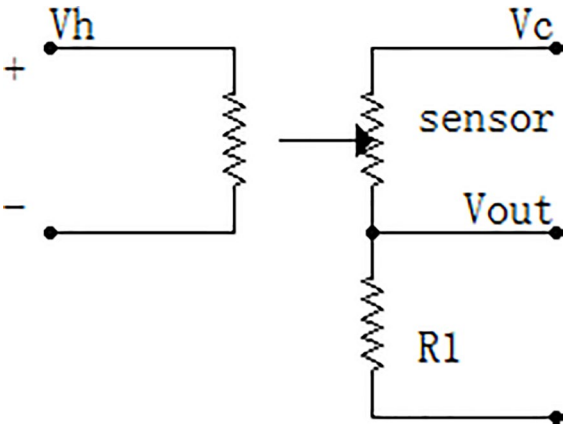

Figure 1. Schematic of gas sensing test circuit

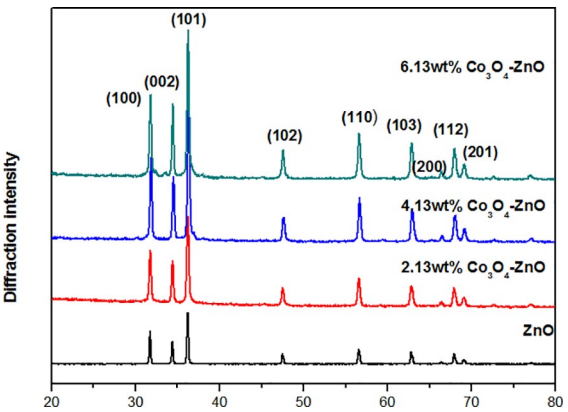

Figure 2. XRD patterns of Co_3O_4-ZnO with different doping concentration

Fig. 3a-d shows SEM images of different doping amounts of Co_3O_4-ZnO samples. It can be seen from the figure that the sample is a hexagonal prism structure, and the Co-doped ZnO material shows a rough and porous structure. Especially when the doping amount is 4.13wt%, the particles of the sample are more uniform and the surface is looser and more porous, and these changes in microscopic morphology caused by doping facilitate the adsorption and desorption of gases. It can be seen from Fig. 4 that the average crystal grain size of Co_3O_4-ZnO is significantly smaller than the average crystal grain size of pure ZnO, and the doping of Co can inhibit the agglomeration of crystal grains and limit the further growth of ZnO crystal grains.

X-ray photoelectron spectroscopy (XPS) was used to characterize and analyze the surface composition and structure of 4.13wt% Co_3O_4-ZnO sample. Fig. 5a shows the Zn 2p spectrum, there were two symmetric peaks in the spectra. One centered at 1020.9 eV corresponded to a Zn $2p_{3/2}$ configuration and another one centered at 1044.0 eV was assigned to a Zn $2p_{1/2}$ configuration [12]. The energy difference between these two peaks is 23.1 eV, which is consistent with the corresponding value of the standard ZnO nanoparticles [13], indicating that the Zn in the sample is in the +2 valence state. Fig. 5b shows the O1s spectrum of 4.13wt% Co_3O_4-ZnO sample. The peak centered at 529.9 eV should be assigned to surface lattice oxygen (Olat), the peak at 531.3eV could be generated by the oxygen species adsorbed on the ZnO surface [14]. Fig. 5c shows the $Co2p_{3/2}$ spectrum of 4.13wt% Co_3O_4-ZnO sample. According to the literature [15], the sample decomposition Co 2p spectrum includes the contributions of Co^{3+} and Co^{2+} and Co^{2+} satellites. Comparing the sample's $Co2p_{3/2}$ binding energy with standard spectra [15,16], we can designate the main peak near 779.9 eV as the $Co^{3+}{}_{3/2}$ configuration, and the other main peak near 781.2 eV as $Co^{2+}{}_{3/2}$ configuration. The small peak at 786.5 eV is the Co^{2+} rocking satellite peak. The surface area ratio of $Co2p_{3/2}$ peaks of Co^{3+} and Co^{2+} is close to 2, corresponding to the formula $Co^{2+}(Co^{3+})_2O_4$ [17].

The results in Fig. 6 indicate the elemental spatial distribution of 4.13wt% Co_3O_4-ZnO nanocomposites.

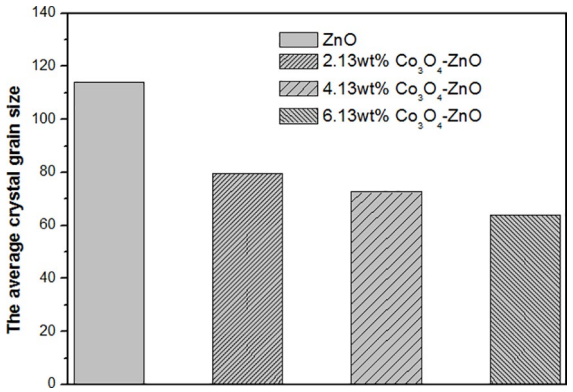

Figure 4. The average crystal grain size of four samples in SEM images

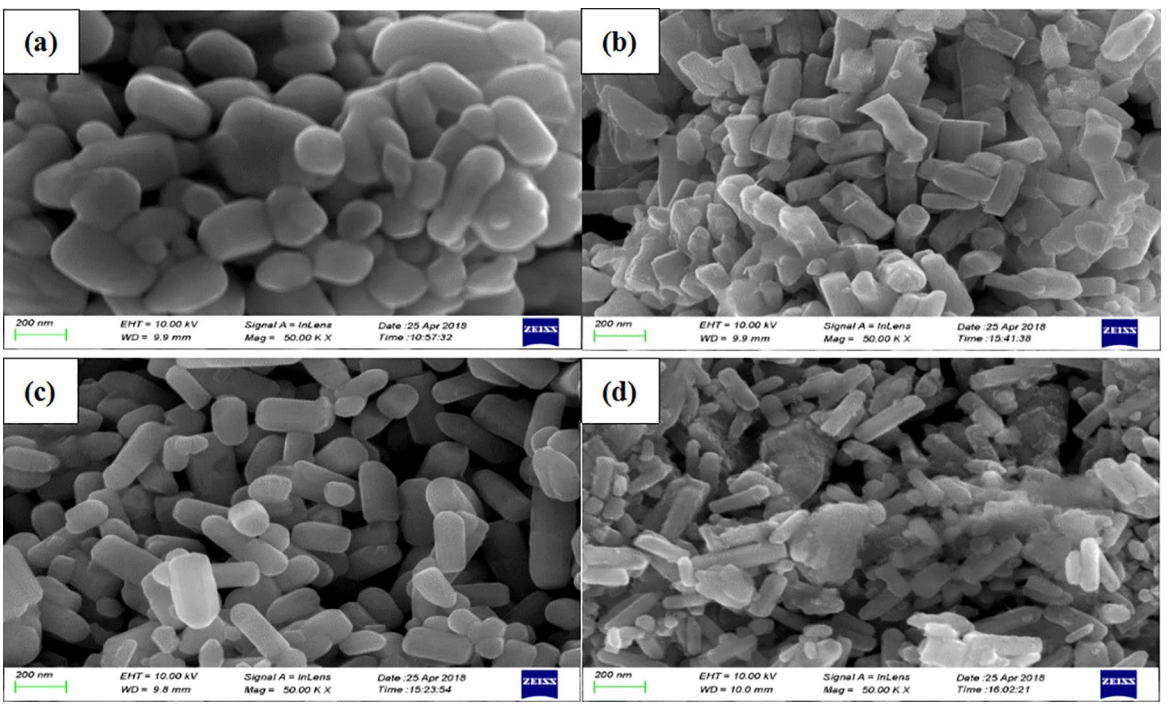

Figure 3. SEM images of Co_3O_4-ZnO nanocomposites with different doping concentration **a)** ZnO **b)** 2.13wt% Co_3O_4-ZnO **c)** 4.13wt% Co_3O_4-ZnO **d)** 6.13wt% Co_3O_4-ZnO

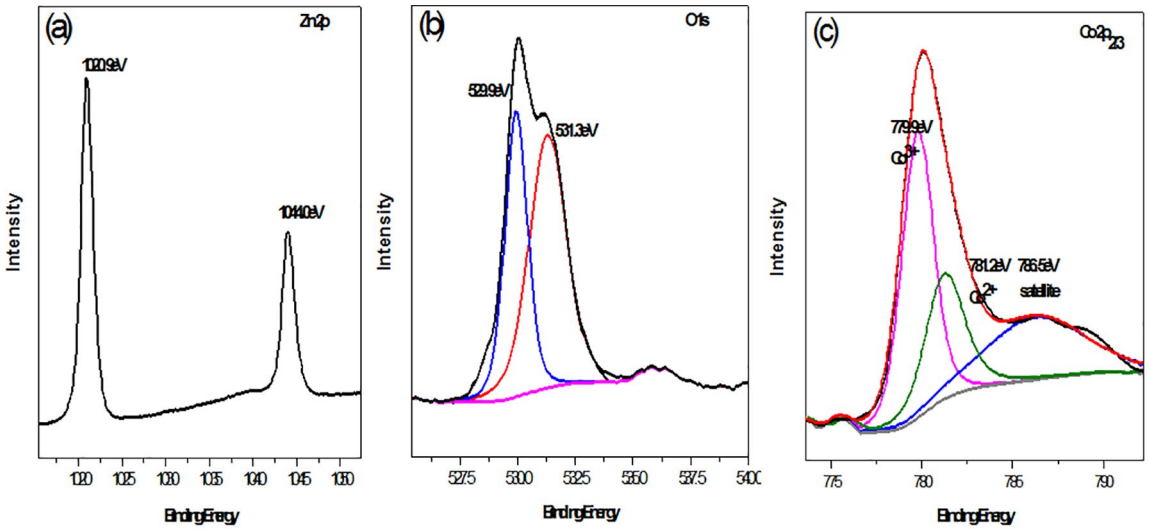

Figure 5. Zn 2p **(a),** O 1s **(b)** and Co $2p_{2/3}$ **(c)** XP spectra of 4.13wt% Co_3O_4-ZnO sample

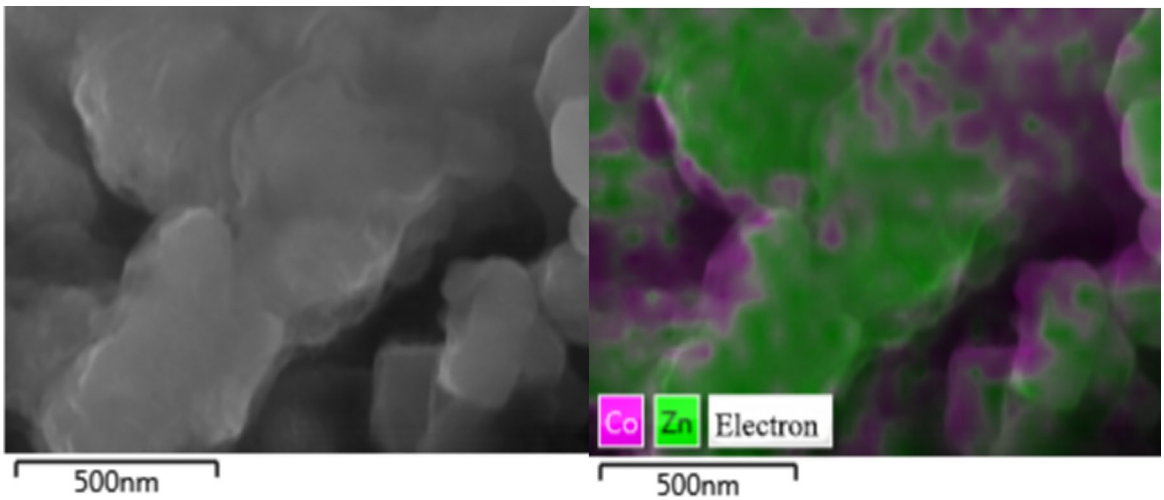

Figure 6. The EDS layered image pattern of 4.13wt% Co_3O_4-ZnO nanocomposites

4.13wt% Co_3O_4-ZnO nanocomposites have agglomerated cobalt-containing particles around their dispersed ZnO, which may be Co_3O_4. Co_3O_4 particles are fully exposed to ZnO and forms P-N heterojunction contact.

3.2 Gas sensitive properties of Co_3O_4-ZnO P-N heterostructure nanocomposites

The sensitivity of ZnO with different doping concentrations was studied by using acetone as the gas to be tested at room temperature (30ºC). Fig. 7a shows the response and recovery curves of four doping concentrations pure ZnO, 2.13wt% Co_3O_4-ZnO, 4.13wt% Co_3O_4-ZnO, and 6.13wt% Co_3O_4-ZnO to 100 ppm acetone. The sensitivity are 6.5, 12.16, 24.36, and 14.22, respectively, indicating that doping Co_3O_4 can improve the sensitivity of ZnO sensor. Compared with undoped ZnO sensors (16 and 7 s, respectively), the response and recovery time of the 4.13wt% Co_3O_4-ZnO sample to 100 ppm acetone (Fig. 7b) were also only 4 seconds and 3 seconds, respectively. The results show that the addition of Co_3O_4 can reduce the response and recovery time of ZnO sensors. When Co_3O_4 is doped in ZnO, the band tail of the Co_3O_4 energy band enters the valence band of ZnO, which makes the band gap narrower and the electrons more prone to transition. Moreover, the addition of Co_3O_4 makes the surface of the sample more loose and porous, providing more active sites for the adsorption of gas molecules and oxygen molecules, thereby improving sensitivity.

However, the sensitivity will decrease when the doping concentration is too high. The possible reason for sensitivity reduction is that ZnO has less contact with oxygen or target gas. The barrier height and resistivity will increase as the additional Co_3O_4 accumulates in the lattice gap or grain boundary of ZnO which hinders the contact[18]. Another possible reason will be discussed later.

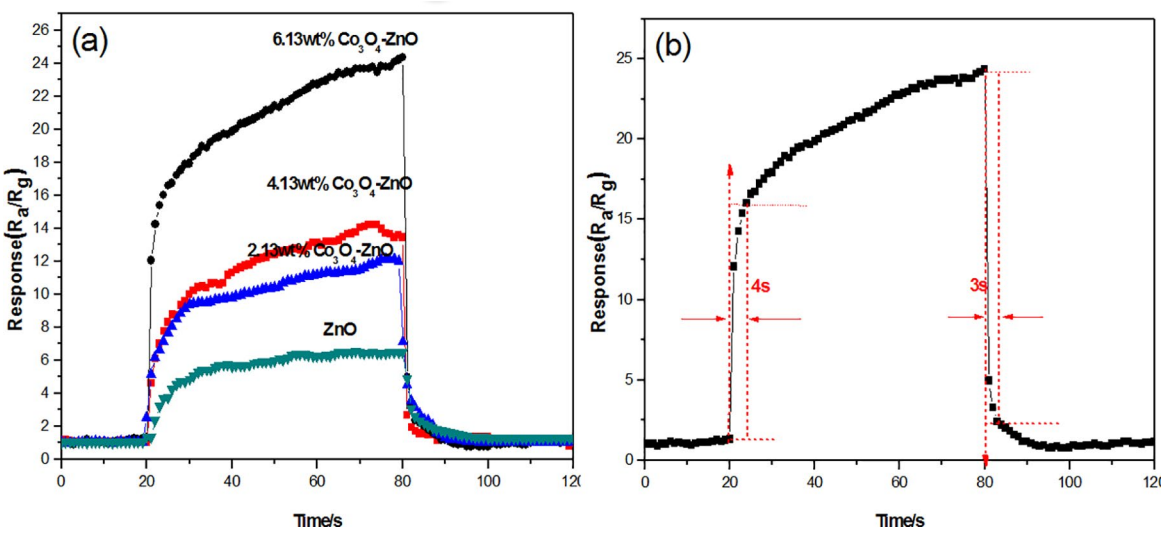

Figure 7. Response and recovery curves for 100 ppm acetone at an operating temperature of 30ºC **a)** Samples of four different doping concentrations **b)** 4.13wt% Co_3O_4-ZnO sample

Fig. 8 depicts the responses of pure ZnO sample and 4.13wt% Co_3O_4-ZnO sample to 100 ppm acetone at 30ºC as well as other gases such as toluene, ammonia, ethylene glycol, and methanol. And the gas sensing properties are shown in Table 1.

It can be easily seen that the 4.13wt% Co_3O_4-ZnO sample always shows a higher response than the pure ZnO in all cases. Its response to acetone is 24.36. It is higher than other gases and shows good selectivity to acetone.

Fig. 9 shows the transient response and recovery curves of 4.13wt% Co_3O_4-ZnO sensor for different concentrations of acetone at an operating temperature of 30ºC. It can be seen from the figure that as the acetone concentration increases, the sensor response value also increases, and when the acetone concentration is as low as 10 ppm, there is also a significant response with a response value of 2.55.

The long-term stability of ZnO and Co_3O_4-ZnO samples to 100 ppm acetone was tested at an operating temperature of 30ºC (Fig. 10). The results show that both sensors have good long-term stability. Compared to the previously reported sensing properties of Co_3O_4-ZnO materials (Table 2), low operating temperatures and relatively high sensitivity make this work very valuable.

3.3 Photoelectric gas sensing properties of Co_3O_4-ZnO P-N heterostructure nanocomposites

In order to study optical properties, diffuse reflectance spectra of pure ZnO and 4.13wt% Co_3O_4-ZnO were measured in the wavelength range of 220-850 nm, as shown in Fig. 11. It can be seen that the absorption of visible light by 4.13wt% Co_3O_4-ZnO is greater than that of pure ZnO.

The energy gap was calculated by kubelka-Munk formula. (Give a graph:[$F(R)\times E]^{1/2}$-E, $F(R)$ is the kubelka-Munk function, $F(R)=(1-R)^2/2R$, R is the reflectivity; E is the energy, $E=1240/\lambda$, the unit is eV; lengthen the part of line in the curve, intersecting with the X axis, the point is the value of energy gap.) As shown in Fig. 12, the band gap energies estimated from the intercept of the tangents to the plots are 3.15eV and 2.19eV for pure ZnO and 4.13wt% Co_3O_4-ZnO nanocomposites, respectively. It indicates that the incorporation of Co_3O_4 leads to a narrow band gap of the material. Since electronic transitions require the effect of thermal excitation, sensors made of materials with narrower band gaps have lower operating temperatures. In addition, reducing the width of the band gap can increase the utilization of visible light.

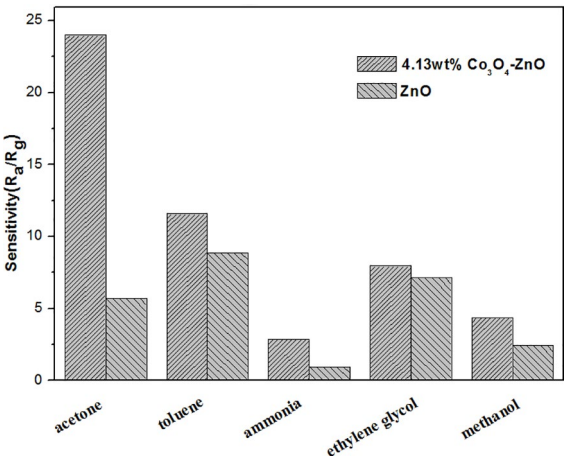

Figure 8. Selectivity of the 4.13wt% Co_3O_4-ZnO and pure ZnO sample to 100 ppm of various gases at 30ºC

In order to investigate the influence of illumination conditions on the gas sensing properties of the components, Co_3O_4-ZnO samples with different doping amounts were irradiated with visible light with a wavelength greater than 420 nm, and their sensitivity to acetone (100 ppm)

Table 1. Gas sensing properties of 4.13wt% Co_3O_4-ZnO and puer ZnO to different gases (100 ppm)

Target gas	Gas response(S)		Response time/s		Recovery time/s	
	4.13wt% Co_3O_4-ZnO	ZnO	4.13wt% Co_3O_4-ZnO	ZnO	4.13wt% Co_3O_4-ZnO	ZnO
Acetone	24.36	6.50	4	16	3	7
Toluene	11.58	8.85	4	14	2	8
Ammonia	2.87	0.96	6	22	6	26
Ethylene glycol	7.96	7.16	5	11	4	15
Methanol	4.34	2.45	7	19	2	15

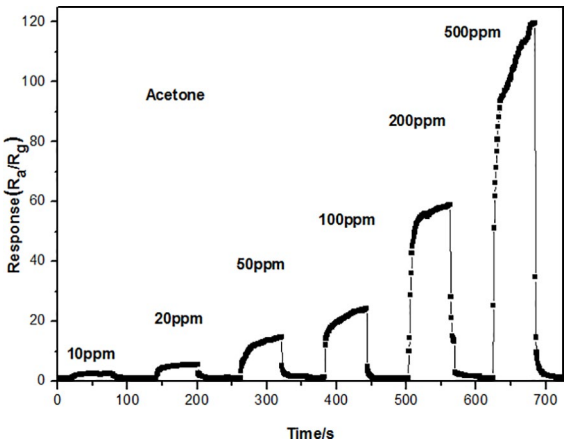

Figure 9. Transient response and recovery curves of 4.13wt% Co_3O_4-ZnO sample for different concentrations of acetone

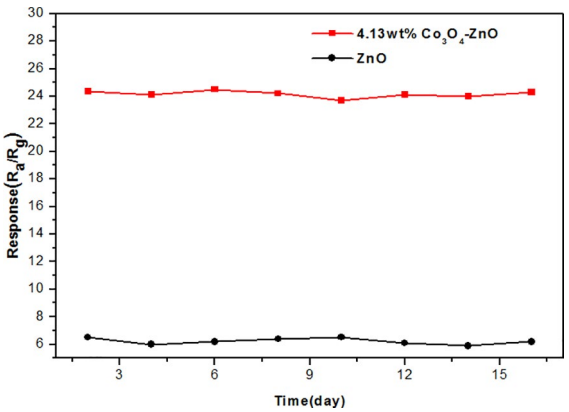

Figure 10. Long-term stability of the ZnO and 4.13wt% Co_3O_4-ZnO to 100 ppm acetone at 30 ºC

was tested. The result is shown in Fig. 13. Clearly, visible light illumination significantly increases the gas response of the gas sensing material, and the incorporation of Co_3O_4 results in a significant increase in photovoltaic gas sensing performance. In particular, when the doping amount of Co_3O_4 is 4.13wt%, the photoexcitation effect reaches the best with 37.21 gas response

Fig. 14 shows gas-sensing curves of pure ZnO samples prepared with and without visible light exposureat for 100 ppm acetone at an operating temperature of 30ºC. It can be seen from the figure that the response time of pure ZnO gas sensitive material under visible light irradiation is greatly reduced compared with pure ZnO gas sensitive material without visible light irradiation, but the sensitivity is not significantly improved. This is due to defects in ZnO, such as Zn vacancies, oxygen vacancies, Zn gaps, and oxygen gaps [22,23].

When visible light is turned on, electrons will be excited by defects, and the electrons generated will reach the conduction band of ZnO, resulting in a decrease in response time. At the same time, the height of the grain boundary barrier will lower and the sensitivity will increase. However, since the amount of electrons excited by visible light associated with weak defects is limited, the sensitivity of pure ZnO under visible light irradiation is very small. When the acetone gas is exhausted, the response cannot immediately return to the initial value. This is because the recombination probability and rate of electrons and holes in pure ZnO are slow, resulting in an increase in recovery time.

Table 2. Sensing performances of Co_3O_4-ZnO gas sensors reported in literatures to VOCs.

Materials	Gas	Concentration /ppm	Temperature /ºC	Response (S)	References
mesoporous ZnO/ Co_3O_4 microspheres	acetone	50	275	29	[19]
Pd@Co_3O_4-ZnO	ethanol	200	240	54	[20]
porous ZnO/Co_3O_4 nanocomposites	acetone	1	275	15.17	[21]
Co_3O_4/ZnO nanocomposites	formaldehyde	100	170	20	[11]
Co_3O_4-ZnO core-shell nanofibers	formaldehyde (acetone)	100	220	5.1(22)	[9]
Co_3O_4-ZnO P-N heterostructure nanomaterials	**acetone**	**100**	**30**	**24.36**	**This work**

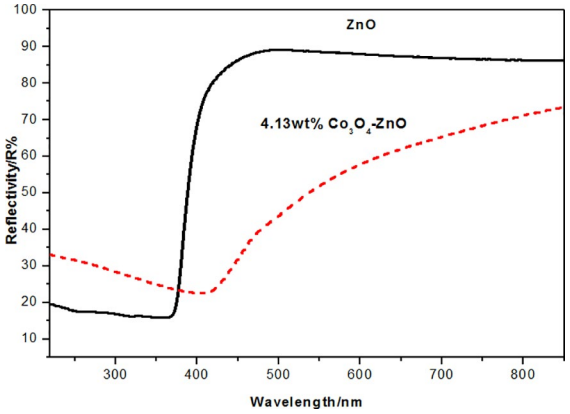

Figure 11. Reflectance spectrum of pure ZnO and 4.13wt% Co_3O_4-ZnO

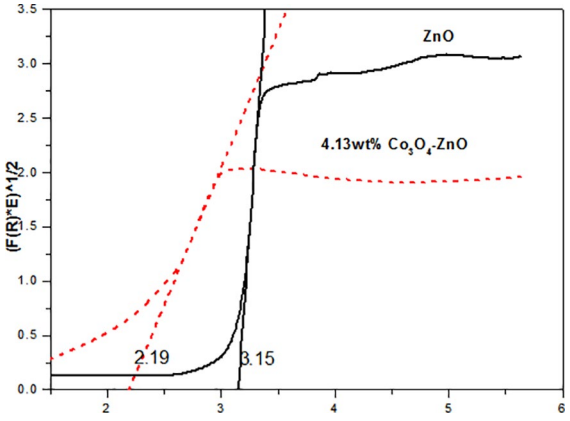

Figure 12. Energy band gap of pure ZnO and 4.13wt% Co_3O_4-ZnO

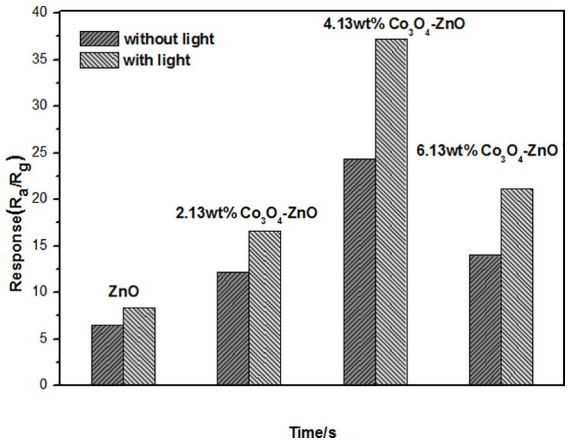

Figure 13. Sensitivity of Co_3O_4-ZnO sample with and without light

Fig. 15 compares the gas sensitivity curves for 4.13wt% Co_3O_4-ZnO with and without visible light illumination. Compared with no visible light irradiation, the gas response of 4.13wt% Co_3O_4-ZnO to the 100ppm acetone with visible light irradiation is significantly improved. The reason is that compared with pure ZnO, the band gap of 4.13wt% Co_3O_4-ZnO sample is narrower and the utilization of visible light is higher. In addition, the surface morphology of 4.13wt% Co_3O_4-ZnO is loose and porous, and the more pores, the more visible light the material captures [24].

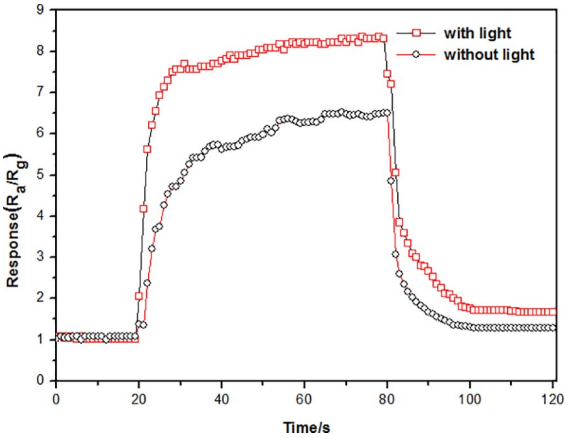

Figure 14. Recovery curve of pure ZnO in response to 100 ppm acetone with and without visible light exposure

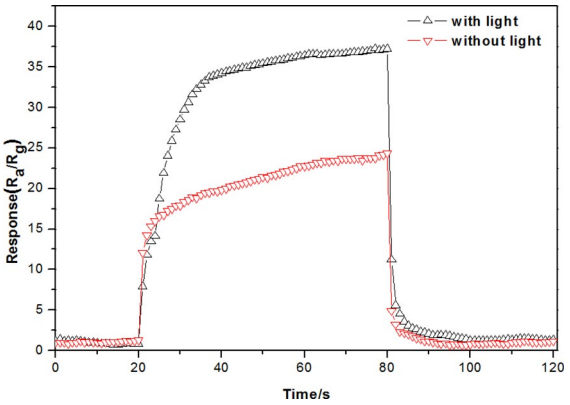

Figure 15. Recovery curve of 4.13wt% Co_3O_4-ZnO in response to 100 ppm acetone with and without visible light

4. Gas Sensing Mechanism

Co_3O_4 is p-type semiconductor withnarrow band gap energy of 1.6 eV and work function of 6.1 eV. As an n-type semiconductor, ZnO has wide band gap energy (3.37 eV) and work function of 5.2 eV at near room temperature. This can be seen from Fig. 16. When Co_3O_4 nanoparticles are adorned onto the surface of ZnO nanoparticles, due to Fermi level-mediated charge transfer[8,25,26], will lead to the for-mation of a P-N heterojunction at the interface between the p-Co_3O_4 nanoparticles and n-ZnO nanoparticles[27,28]. The electrons in ZnO will be transferred to the Co_3O_4 nanoparticles, which significantly reduces the charge conduction channel and results in a higher resistance state than pure ZnO.

When the ZnO nanoparticles are heated by exposure to air, oxygen molecules are adsorbed on the surface of the ZnO nanoparticles. These chemisorbed oxygen trap electrons from the ZnO conduction band and form adsorbed oxygen

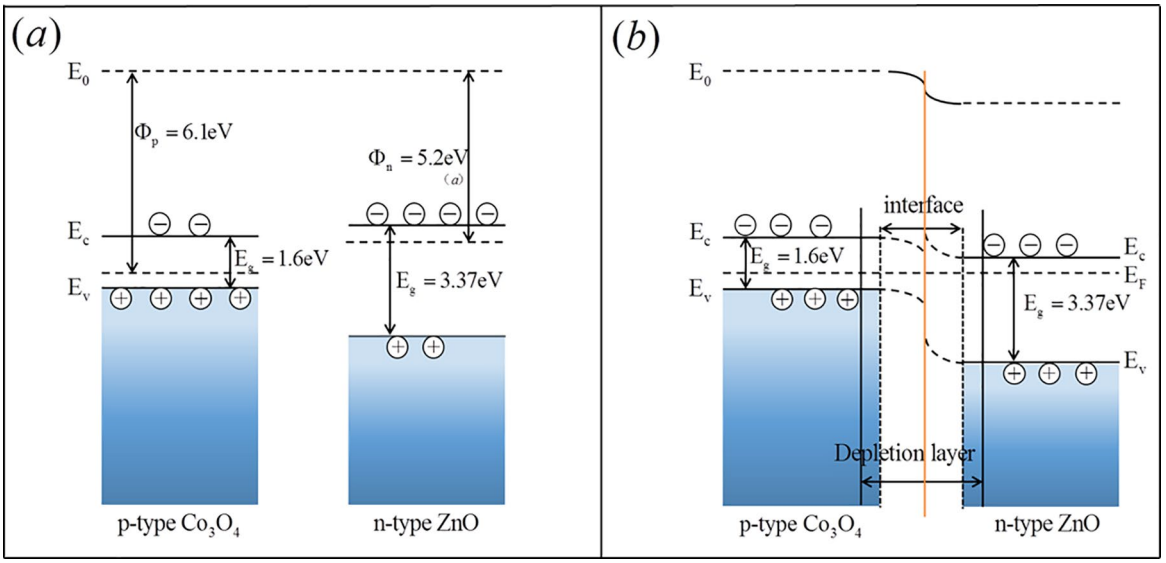

Figure 16. a) The energy band diagram of p-Co_3O_4 and n-ZnO **b)** the energy band diagram for P-N junction of Co_3O_4-ZnO nanocompoosites with a depletion layer at the interface

ions, resulting in changes in carrier concentration and material resistance. Due to the low operating temperature of the sensor, oxygen ions mainly exist in the form of O_2^-. The adsorption process for n-type ZnO is as follows [29,30]:

$$O_2(g) \rightarrow O_2(ads) \tag{2}$$

$$O_2(ads) + e^- \rightarrow O_2^-(ads) \tag{3}$$

For Co_3O_4, since it is a p-type semiconductor, the adsorption process is as follows[9]:

$$O_2(g) \rightarrow O_2^-(ads) + h_* \tag{4}$$

Obviously, the capture of electrons in ZnO leads to an increase in the barrier between ZnO nanoparticles, while the accumulation of holes in Co_3O_4 leads to a decrease in barrier. However, since Co_3O_4 is less in cobalt-doped ZnO, the conductivity of the ZnO and p-n heterojunction plays a major role. The resistance of pure ZnO and 4.13wt% Co_3O_4-ZnO in air at room temperature was 18384 ohms and 24689 ohms, respectively.

When the Co_3O_4-ZnO sensor is exposed to a certain concentration of acetone gas, the gas is oxidized by the negatively charged oxygen ions, and the electrons trapped by the O_2^- ion are automatically released back to the conduction band of ZnO, resulting in an increase in electron concentration in the conduction band and a significant decrease in the sensor resistance, the reaction occurred as follows:

$$(CH_3)_2CO(g) + 4O_2^-(g) \rightarrow 3CO_2(g) + 3H_2O(l) + 4e^- \tag{5}$$

In addition, the acetone gas also releases electrons into the p-type Co_3O_4 nanoparticles, recombines with their holes, thinning the interface depletion layer, and lowering the interface barrier height (Fig. 17a). Therefore, the resistance of the Co-doped zinc oxide based sensor is further reduced than that of the original ZnO sensor.

It is worth noting that after the acetone gas is introduced, part of the Co^{3+} is reduced to Co^{2+}[31]. The reaction mechanism is as follows:

$$2Co_3O_4 + (CH_3)_2CO(g) + 3O_2(g) \rightarrow 6CoO + 3CO_2(g) + H_2O(l) \tag{6}$$

In the gas detection process, acetone molecules are directly oxidized on the surface of Co_3O_4 particles. This leads to the decrease in the quantity of acetone molecules which can react with the oxygen chemisorbed on ZnO surface, and consequently to the decrease in sensor signal of Co_3O_4-ZnO comparing with pure ZnO. However, the introduction of the Co_3O_4 impurity level greatly enhances the carrier concentration, and the reduction in the sensor signal will be offset by the rapid increase in carrier concentration. In addition, Co doping forms a new degeneracy band, resulting in a band gap narrowing effect, which makes it easier for electrons to excite from the valence band to the conduction band, adsorbing more surface oxygen species, leading to higher Ra.

With the increase of the amount of Co_3O_4 doping, Co_3O_4 will be transformed into the main conduction path. At this moment, the holes accumulation of Co_3O_4 in the air will not be ignored, which may cause the performance of the sensor

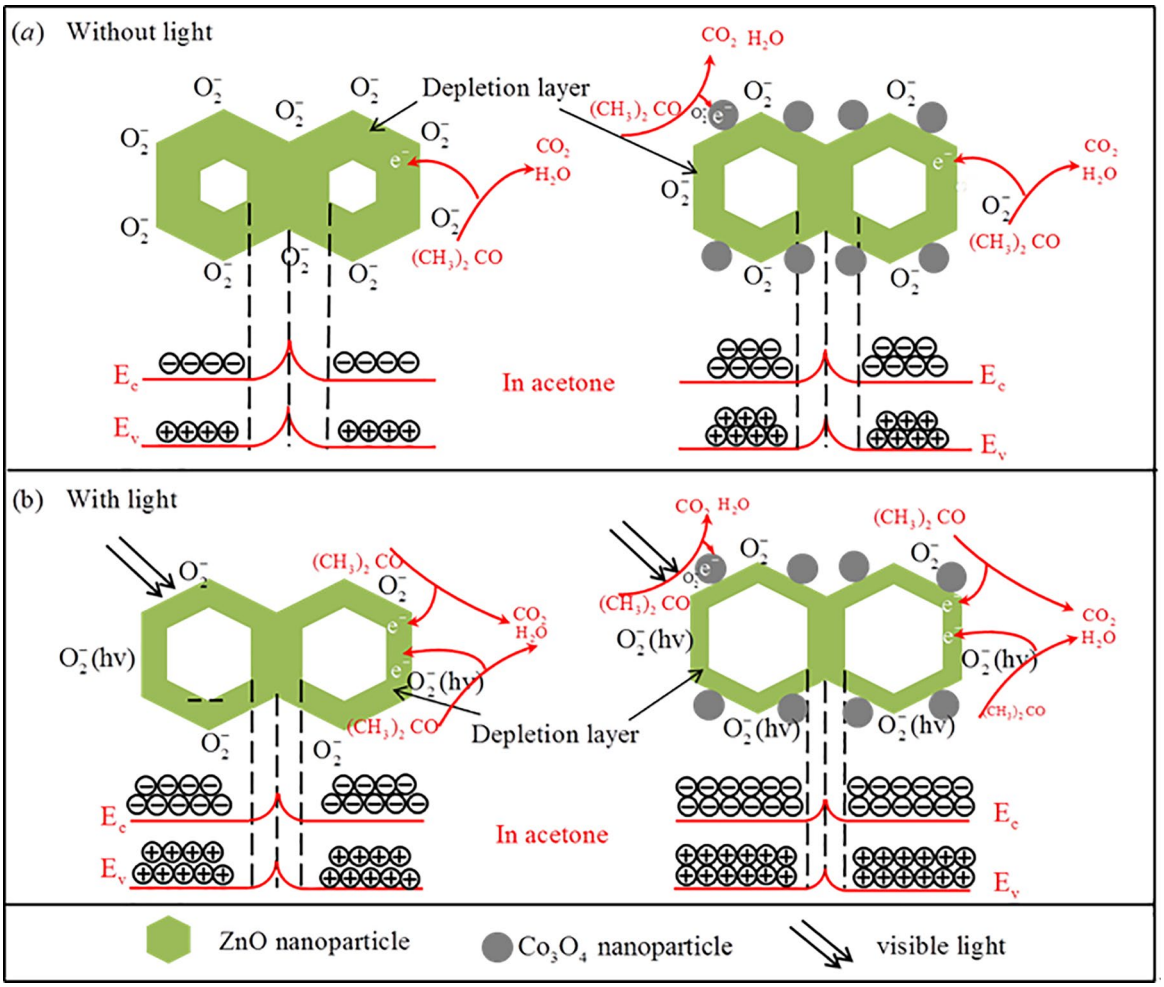

Figure 17. The scheme of P-N heterojunction models of both ZnO and Co_3O_4-ZnO nanocompoosites with and without visible light irradiation

to decrease. Therefore, the loading of Co_3O_4 nanoparticles should be strictly controlled to obtain better sensor response.

When visible light is irradiated on the surface of the sensor, the band gap of the Co_3O_4-ZnO sample is greatly reduced due to the addition of Co_3O_4[32]. Therefore, Co_3O_4-ZnO samples are more easily excited by visible light under visible light irradiation. High-energy photons are absorbed by the Co_3O_4-ZnO sample and produce electron-hole pairs. As the following equation shows:

$$h\nu \rightarrow h^+ + e^- \tag{7}$$

This process increases the carrier concentration and the conductivity of the nanocomposite. With the bandgap matching and influence of the heterojunction between Co_3O_4 and ZnO, the photogenerated electrons in the Co_3O_4-ZnO sample will migrate into ZnO, while the photogenerated holes will transfer to Co_3O_4, thus leading to the broadening of the Co_3O_4-ZnO interface depletion layer, and the resistance of the Co_3O_4-ZnO sensor is further increased. In addition, photogenerated electrons diffuse to the surface of ZnO and react with the oxygen molecules adsorbed on the surface. The reaction is as follows [33]:

$$O_2 + e^-(h\nu) \rightarrow O_2^-(h\nu) \tag{8}$$

This process effectively suppresses the recombination between photo-generated carriers and produces more photo-oxidizing ions than pure ZnO. When exposed to acetone gas, acetone reacts with adsorbed oxygen ions and photooxygen ions on the ZnO surface. The electrons generated by the reaction are reintroduced into the conduction band of ZnO.

$$\begin{aligned}&(CH_3)_2CO(g) + 4O_2^-(h\nu) \rightarrow \\ &3CO_2(g) + 3H_2O(l) + 4e^-\end{aligned} \tag{9}$$

This can be seen from Fig. 17b. Therefore, this interfacial charge transfer can effectively promote the separation of electrons and holes, and further increase the number of electrons in ZnO, leading to more significant changes in resistance and improved sensitivity.

5. Conclusion

In summary, the heterostructure Co_3O_4-ZnO thick film was successfully prepared by sol-gel method, and its gas sensitivity was studied. The doping of Co_3O_4 leads to an increase in the crystallinity of the Co_3O_4-ZnO sample and the formation of a p-n heterojunction, which leads to its more pronounced modulation of the resistance at the surface of the material. In the experiment, it is observed that Co_3O_4--doped ZnO thick-film sensors show higher sensitivity to acetone and better selectivity than undoped ZnO thick-film sensors at low temperatures. The sensitivity of 4.13wt% Co_3O_4-ZnO to 100 ppm acetone is 3.6 times higher than that of pure ZnO and the response recovery time is also reduced at room temperature 30ºC. In addition, optical excitation can enhance gas sensing characteristics and lower operating temperatures. The sensitivity of 4.13wt% Co_3O_4-ZnO under visible light was 1.52 times higher than that without visible light irradiation. Therefore, the doping of Co_3O_4 and the visible light illumination have a synergistic effect in improving the gas sensing characteristics of the sensor, further improving the sensitivity of the sensor and reducing the operating temperature of the element.

6. Acknowledgements

This work was supported by the National Natural Science Foundation of Tianjin (No. 17JCTPJC54500). The authors are also grateful to the Key Laboratory of Electronic Materials and Devices of Tianjin, China.

7. References

1. Schmidt-Mende L, MacManus-Driscoll JL. ZnO - nanostructures, defects, and devices. *Materialstoday*. 2007;10(5):40-48.

2. Barsan N, Koziej D, Weimar U. Metal oxide-based gas sensor research: How to? *Sensors and Actuators B: Chemical*. 2007;121(1):18-35.

3. Pisarev RV, Pavlov VV, Kalashnikova AM, Moskvin AS. Near-band gap electronic structure of the tetragonal rare-earth cuprates R_2CuO_4, and the bismuth cuprate Bi_2CuO_4. *Physical Review B*. 2010;82(22):224502.

4. Neri G, Bonavita A, Rizzo G, Galvagno S, Capone S, Siciliano P. Methanol gas sensing properties of CeO_2-Fe_2O_3 thin films. *Sensors and Actuators B: Chemical*. 2006;114(2):687-695.

5. Hastir A, Kohli N, Singh RC. Temperature dependent selective and sensitive terbium doped ZnO nanostructures. *Sensors and Actuators B: Chemical*. 2016;231:110-119.

6. Xu Q, Ju D, Zhang Z, Yuan S, Zhang J, Xu H, et al. Near room-temperature triethylamine sensor constructed with CuO/ZnO P-N heterostructural nanorods directly on flat electrode. *Sensors and Actuators B: Chemical*. 2016;225:16-23.

7. Rambu AP, Iftimie N, Nica V, Dobromir M, Tascu S. Efficient methane detection by Co doping of ZnO thin films. *Superlattices & Microstructures*. 2015;78:61-70.

8. Wang L, Kang Y, Wang Y, Zhu B, Zhang S, Huang W, et al. CuO nanoparticle decorated ZnO nanorod sensor for low-temperature H2S detection. *Materials Science & Engineering: C*. 2012;32(7):2079-2085.

9. Gao X, Li F, Wang R, Zhang T. A formaldehyde sensor: Significant role of p-n heterojunction in gas-sensitive core-shell nanofibers. *Sensors and Actuators B: Chemical*. 2018;258:1230-1241.

10. Peng C, Guo J, Yang W, Shi C, Liu M, Zheng M, et al. Synthesis of three-dimensional flower-like hierarchical ZnO nanostructure and its enhanced acetone gas sensing properties. *Journal of Alloys and Compounds*. 2016;654:371-378.

11. Liu Y, Zhu G, Chen J, Xu H, Shen X, Yuan A. Co_3O_4/ZnO nanocomposites for gas-sensing applications. *Applied Surface Science*. 2013;265:379-384.

12. Choi SW, Katoch A, Sun GJ, Kim JH, Kim SH, Kim SS. Dual functional sensing mechanism in SnO_2-ZnO core-shell nanowires. *ACS Applied Materials & Interfaces*. 2014;6(11):8281-8287.

13. Moulder JF, Chastain J, King RC. Handbook of X-ray Photoelectron Spectroscopy: A Reference Book of Standard Spectra for Identification and Interpretation of XPS Data. *Eden Prairie: Physical Electronics*; 1995.

14. Chen M, Wang X, Yu YH, Pei ZL, Bai XD, Sun C, et al. X-ray photoelectron spectroscopy and auger electron spectroscopy studies of Al-doped ZnO films. *Applied Surface Science*. 2000;158(1-2):134-140.

15. Tan BJ, Klabunde KJ, Sherwood PMA. XPS studies of solvated metal atom dispersed (SMAD) catalysts. Evidence for layered cobalt-manganese particles on alumina and silica. *Journal of the American Chemical Society*. 1991;113(3):855-861.

16. McIntyre NS, Cook MG. X-ray photoelectron studies on some oxides and hydroxides of cobalt, nickel, and copper. *Analytical Chemistry*. 1975;47(13):2208-2213.

17. Fu L, Liu Z, Liu Y, Han B, Hu P, Cao L, et al. Beaded Cobalt Oxide Nanoparticles along Carbon Nanotubes: Towards More Highly Integrated Electronic Devices. *Advanced Materials*. 2005;17(2):217-221.

18. Ng ZN, Chan KY, Low CY, Kamaruddin SA, Sahdan MZ. Al and Ga doped ZnO films prepared by a sol-gel spin coating technique. *Ceramics International*. 2015;41(Suppl 1):S254-S258.

19. Zhang L, Jing X, Liu J, Wang J, Sun Y. Facile synthesis of mesoporous ZnO/Co3O4 microspheres with enhanced gas-sensing for ethanol. *Sensors and Actuators B: Chemical*. 2015;221:1492-1498.

20. Sun Y, Wang Z, Wang W, Li G, Li P, Lian K, et al. Electrospinning preparation of Pd@ Co_3O_4-ZnO composite nanofibers and their highly enhanced VOC sensing properties. *Materials Research Bulletin*. 2019;109:255-264.

21. Xiao J, Diao K, Zheng Z, Cui X. MOF-derived porous ZnO/Co_3O_4, nanocomposites for high performance acetone gas sensing. *Journal of Materials Science: Materials in Electronics*. 2018;29(10):8535-8546.

22. Jeong D, Kim K, Park SI, Kim YH, Kim S, Kim SI. Characteristics of Ga and Ag-doped ZnO-based nanowires for an ethanol gas sensor prepared by hot-walled pulsed laser deposition. *Research on Chemical Intermediates*. 2014;40(1):97-103.

23. Sarkar D, Khan GG, Singh AK, Mandal K. Enhanced Electrical, Optical, and Magnetic Properties in Multifunctional ZnO/a-Fe_2O_3 Semiconductor Nanoheterostructures by Heterojunction Engineering. *Journal of Physical Chemistry C*. 2012;116(44):23540-23546.

24. Li Y, Li DL, Liu JC. Optical and gas sensing properties of mesoporous hollow ZnO microspheres fabricated via a solvothermal method. *Chinese Chemical Letters*. 2015;26(3):304-308.

25. Miller DR, Akbar SA, Morris PA. Nanoscale metal oxide-based heterojunctions for gas sensing: A review. *Sensors and Actuators B: Chemical*. 2014;204:250-272.

26. Xu Z, Duan G, Li Y, Liu G, Zhang H, Dai Z, et al. CuO-ZnO Micro/Nanoporous Array-Film-Based Chemosensors: New Sensing Properties to H_2S. *Chemistry - A European Journal*. 2014;20(20):6040-6046.

27. Ge L, Jing X, Wang J, Wang J, Jamil S, Liu Q, et al. Trisodium citrate assisted synthesis of ZnO hollow spheres via a facile precipitation route and their application as gas sensor. *Journal of Materials Chemistry*. 2011;21(29):10750-10754.

28. Lou Z, Li F, Deng J, Wang LL, Zhang T. Branch-like Hierarchical Heterostructure (a-Fe_2O_3/TiO_2): A Novel Sensing Material for Trimethylamine Gas Sensor. *ACS Applied Materials & Interfaces*. 2013;5(23):12310-12316.

29. Mondal B, Basumatari B, Das J, Roychaudhury C, Saha H, Mukherjee N. ZnO-SnO_2, based composite type gas sensor for selective hydrogen sensing. *Sensors and Actuators B: Chemical*. 2014;194:389-396.

30. Zeng Y, Zhang T, Yuan M, Kang M, Lu G, Wang R, et al. Growth and selective acetone detection based on ZnO nanorod arrays. *Sensors and Actuators B: Chemical*. 2009;143(1):93-98.

31. Rumyantesva MN, Vladimirova SA, Vorobyeva NA, Giebelhaus I, Mathur S, Chizhov AS, et al. p-CoOx/n-SnO_2 nanostructures: New highly selective materials for H_2S detection. *Sensors and Actuators B: Chemical*. 2018;255(Pt 1):564-571.

32. Wang X, Zheng R, Liu Z, Ho HP, Xu J, Ringer SP. Structural, optical and magnetic properties of Co-doped ZnO nanorods with hidden secondary phases. *Nanotechnology*. 2008;19(45):455702.

33. Panda SK, Jacob C. Preparation of transparent ZnO thin films and their application in UV sensor devices. *Solid State Electronics*. 2012;73(14):44-50.